Available online at www.sciencedirect.com

jmr&t Journal of Materials Research and Technology

www.jmrt.com.br

Original Article

Bioinspired composite segmented armour: Numerical simulations

Pedro Miranda[a,*], *Antonia Pajares*[a], *Marc A. Meyers*[b]

[a] *Departamento de Ingeniería Mecánica Energética y de los Materiales, Universidad de Extremadura Escuela de Ingenierías Industriales, Avda. de Elvas s/n, 06006 Badajoz, Spain*

[b] *Depts. of Mechanical and Aerospace Eng. and Nanoengineering, University of California San Diego, La Jolla, CA 92093-0411, United States*

ARTICLE INFO

Article history:
Received 26 June 2018
Accepted 13 September 2018
Available online 16 November 2018

Keywords:
Scaled armour
Ballistic impact
Alumina
Epoxy
Finite element analysis
Bioinspiration

ABSTRACT

Nature has evolved ingenious armour designs, like the flexible carapaces of armadillo and boxfish consisting of hexagonal segments connected by collagen fibres, that serve as bioinspiration for modern ballistic armours. Here, Finite element modelling (FEM) used to analyze the effect of scale geometry and other impact parameters on the ballistic protection provided by a bioinspired segmented ceramic armour. For this purpose, the impact of cylindrical fragment simulating projectiles (FSPs) onto alumina-epoxy non-overlapping scaled plates was simulated. Scale geometrical parameters (size, thickness and shape) and impact conditions (FSP diameter, speed, location) are varied and the amount of damage produced in the ceramic tiles and the final residual velocity of the FSP after the impact are evaluated. It is found that segmentation drastically reduces the size of the damaged area without significantly reducing the ballistic protection in centred impact, provided the tile size is kept over a critical value. Such critical tile size (~20 mm, inscribed diameter, for impacts at 650 m/s) is independent of the scale thickness, but decreases with projectile speed, although never below the diameter of the projectile. Off-centred impacts reduce the ballistic protection and increase the damaged area, but this can be minimized with an appropriate tile shape. In this sense and in agreement with the natural hexagonal tiles of the boxfish and armadillo, hexagonal scales are found to be optimal, exhibiting a variation of ballistic protection—measured as reduction of projectile speed—with impact location under 12%. Design guidelines for the fabrication of segmented protection systems are proposed in the light of these numerical results.

* *Corresponding author.*
E-mail: pmiranda@unex.es (P. Miranda).

https://doi.org/10.1016/j.jmrt.2018.09.007

1. Introduction

Bioinspiration is a rapidly evolving field of scientific inquiry by which the lessons learned from nature are applied to synthetic materials and designs that have performance superior to that of conventional ones. There are amazing success stories, the burr-inspired reversible attachment device Velcro being the best known. Nature has developed, through billions of years of evolution, ingenious solutions that we are only now able to fully comprehend; their use in synthetic designs is an area of increasing research and great potential. Novel bioinspired designs such as the Gecomer, inspired on the gecko feet are being commercialized, and other concepts are constantly being implemented. In the area of protection, nature has used flexible dermal armour; this has occurred, through convergent evolution, in fish, reptiles, and mammals [1]. The study of biological materials, which was at its outset exploratory, is currently being systematized, and eight structural design elements were proposed as motifs that appear in different species but use the same principles. These are classified into fibrous, helical, gradient, layered, tubular, cellular, suture, and overlapping structural design elements [2,3].

In many cases protection from predators is ensured by overlapping structures; fish, reptile, and pangolin (a mammal) scales are a prime example [4–9]. There are also cases where juxtaposed plates are used. The latter situation is observed in two different species: the armadillo [10] and the boxfish [11,12]. Fig. 1 shows the regular arrangement of hexagonal bony plates in the armadillo. They are connected by collagen fibres (Shapey's fibres) that provide a certain degree of flexibility. A similar concept is exhibited for protection of the boxfish (Fig. 2). It is interesting to observe that these two plate armours evolved independently in fish and mammals.

Emulating these natural dermal armours, humans have used segmented or scaled armours—also referred as mosaic, patterned or tiled armours—for the protection of soldiers and their mounts since antiquity. For example, the Roman *lorica segmentata*, consisting of metal strips fastened to internal leather straps, and *lorica squamata*, made of overlapping iron or bronze scales sewn to a fabric backing, were among the most effective armours used by Roman legionaries [13], and similar protection systems are found, among others, in Chinese and Japanese warfare history. Scaled armours, like other metal-based armours, were eventually discarded after the

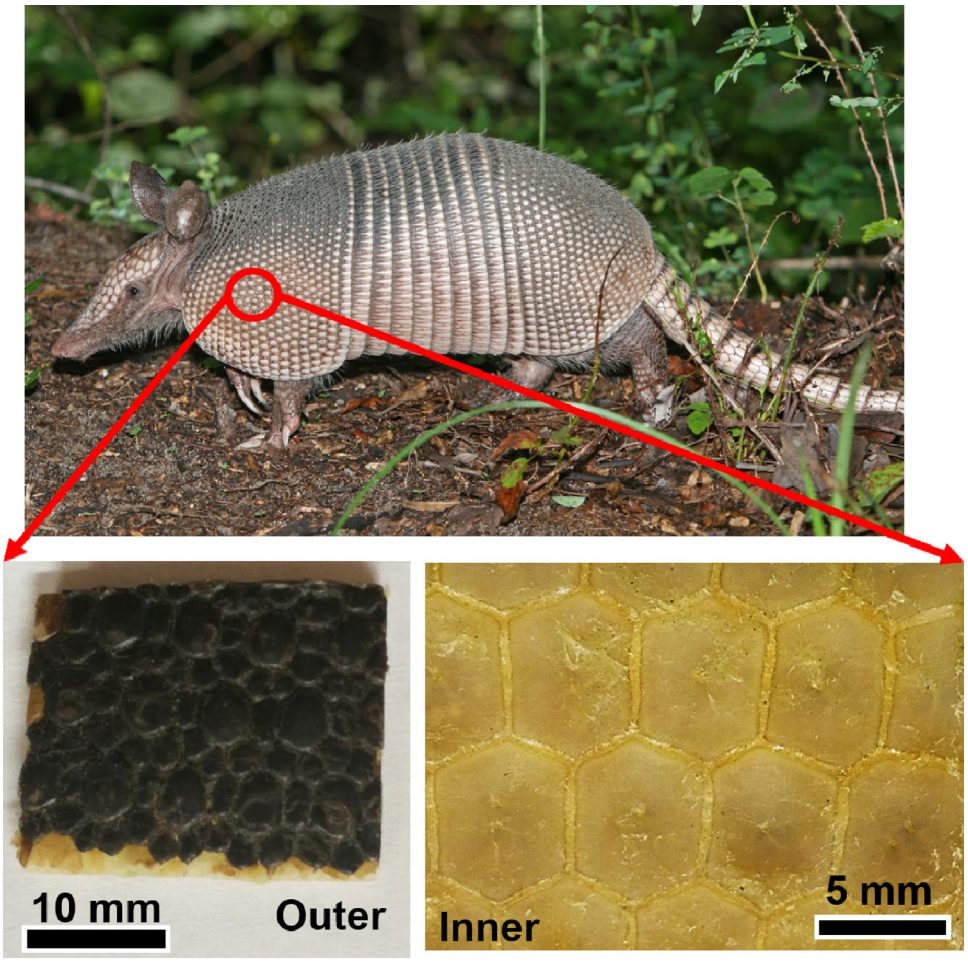

Fig. 1 – Armadillo carapace composed of (bottom right) hexagonal bony segments with approximately 5 mm diameter connected by collagen known as Sharpey's fibres. The surface of the carapace (bottom left) consists of a keratinous layer that ensures impermeability. The keratin layer is also segmented. This configuration provides a balance of flexibility and stiffness required for protection against predators.

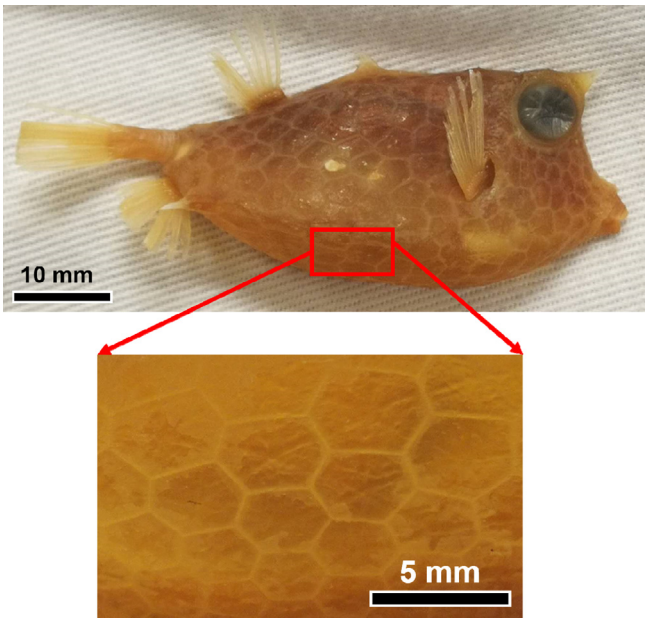

Fig. 2 – Boxfish (*Lactoria cornuta*) carapace consisting of primarily hexagonal hydroxyapatite plates connected by collagen fibres in a complex arrangement. This structure allows for elevated strength of the carapace through redistribution of the force application area under the action of predator teeth.

widespread use of gunpowder, as they were ineffective against ballistic threats.

Metallic body armour was progressively substituted by textile fabrics made from strong fibres like silk (Japan, sXIX) and, eventually, modern organic synthetic fibres of aramid or polyethylene. These modern fabrics (Kevlar®, Nomex®, Twaron®, Dyneema®, Spectra®, Goldflex®, etc.) dominate the production of protective vests, thanks to their high specific strength. However, vests fabricated from ballistic fabrics present some disadvantages that limit their performance under certain conditions. On the one hand, they exhibit relatively limited protection against cutting or stabbing (i.e. impact by sharp objects) [14,15]. And on the other, a substantial level of trauma by impact can still be produced in the wearer due to stress concentration in a very small area [16]. Indeed, NIJ Standard 0101.06 for 'Ballistic Resistance of Body Armor', allows a maximum *backface signature*—i.e. the deformation that a projectile creates behind the armour upon impact—of 44 mm in depth, which could even allow for an internal injury [16]. Even in vests fabricated according to the more stringent European standards, where maximum allowable signature is reduced to 20–25 mm, blunt force trauma injuries are still commonplace. Consequently, the need of providing "multi-threat" protection from cut, stab and ballistic hazards for military and law enforcement agents, and reducing the incidence of backface signature injuries, has resulted in the developments of composite vest and protections. This type of composite armour basically consists of the use of multiple protective layers with complementary functions.

One of the most common strategies to simultaneously improve the ballistic performance of the vests and reduce blunt trauma injuries is to incorporate ceramic elements, usually in the form of a monolithic pectoral plate [17]. Although the incorporation of such plates indeed provides substantial improvements in ballistic protection, it comes at a penalty on vest flexibility, concealability and ergonomics. Thus, the *lorica squamata*, a scaled armour, was preferred by many soldiers. Moreover, such monolithic ceramic plates do not provide a very effective protection against multiple impacts. Indeed, when a projectile impacts the ceramic plate, brittle failure leads to extensive fragmentation of the tile, with the damage spreading over most of or even the entire ceramic surface [18–20]. Obviously, this severely reduces the multi-hit resistance of the armour, especially when no means for retention of the ceramic fragments is used [21].

Since modern-day armours are regularly subjected to fire from automatic weapons, multi-hit protection has become essential. Protection against multiple impacts can be realized in composite (ceramic/textile) vests by keeping as much of the ceramic material as possible intact after each hit. This can be achieved by substituting the monolithic ceramic plates by a mosaic of smaller tiles/scales so that each impact damage affects only a single or, most commonly, a few adjacent tiles [22]. Thus, as a consequence of the limitations of current vest technology, the use of biologically inspired scale armours is being revisited [19,23–26]. However, and unlike most artificial scale armours currently used, natural scales—consisting of a thin mineral (ceramic) surface layer typically made of hydroxyapatite—are joined together by connective collagen-based tissue [27] (Figs. 1 and 2). These soft tissue joints allow the animals to maintain flexibility and motion in spite of the scales' individual rigidity.

Such a combination of organic (polymeric) and inorganic (ceramic) materials offers also interesting prospects for the fabrication of body armours with improved ballistic protection. Most existing bio-inspired scale armours consist of individual segments made of monolithic or composite material with predefined shape and size, held together by a flexible fabric or enveloped between two high tensile strength layers [23,28]. However, laterally bonding the scales together by means of an adhesive might provide certain advantages. On the one hand, it could increase the strength of the plates by sealing existing defects in the surfaces of the ceramic plates [29,30], and preventing the generation of additional damage in service due to lateral contacts between the scales. And on the other, it might help alleviate to some extent the problem of failure by scale tilting when hit close to the edge of a scale [23]. Flexibility of such an adhesively jointed scaled armour, will of course depend on the stiffness and thickness of the selected adhesive.

Despite the potential advantages of such bioinspired segmented armours, there is still very scarce literature [28,31] on the effect of the different geometrical variables (tile size, shape, etc.) on the ballistic performance of such segmented structures. As already mentioned, in order to enhance multi-hit protection it is necessary to reduce the scale size, thus minimizing the unprotected area as tiles are destroyed by preceding impacts. However, reducing the tile size leads to an increase in the interface areal density, which increases the probability of an interface hit. There are some statistical analyses of such probabilities and how they might affect

the segmented armour multi-hit protection as a function of tile size [32,33]. However, those analyses assumed an arbitrary deleterious effect of interfacial hits which has not been evaluated neither by experimental nor numerical means. A reliable evaluation of multi-hit performance of segmented tiles would require knowing how the ballistic protection is affected by the proximity of the impact to the scale edge. Without this knowledge, only crude assumptions can be made. Chintapalli et al. have analyzed the effect of scale size and impact location under quasi-static loading on microperforated glass hexagonal plates [23], and Fejdyś et al. have studied the ballistic performance of scaled composite armours with several geometric configurations [28]. However, to the best of our knowledge there is no systematic study on the effect of all these parameters (size, impact location, scale geometry, etc.) on the ballistic performance of scaled armours.

The present study seeks to redress this deficiency by systematically exploring all these critical design aspects with the aid of finite element simulations. As described in detail in the following section, an adhesively jointed alumina-based segmented plate without any underlying substrate, is used as a model system. Its ballistic performance against impact by a cylindrical fragment simulating projectile is evaluated under varying geometrical conditions including scale size and shape and impact location, among others.

2. Computational model/numerical simulations

2.1. General model description

Finite element simulations were performed using the commercial software ABAQUS/Explicit®, which is appropriate for finding numerical solutions to high speed, non-linear transient problems. A three-dimensional model was used to simulate the impact of a fragment simulating projectile (FSP) onto the centre of an alumina-based scaled plate without any type of backing, as shown in Fig. 3. Fully-restrained (*encastre*) boundary conditions were applied to the lateral surfaces at the perimeter of the ceramic plate. The type of projectile selected is a steel cylinder with a diameter $d = 5.39$ mm and a height $h = 6.17$ mm, yielding a total mass $m = 1.1$ g, which matches one of the standard STANAG specifications for such FSPs [34]. Although simulating shrapnel is in itself of great interest for personnel armour development, this particular FSP was selected because it is similar in mass and diameter to a .22 calibre bullet. Besides, the selection of a cylindrical shape simplifies analysis by reducing the number of geometrical variables in the model. FSP initial velocity was, in general, set at 650 m/s, corresponding to the highest protection level (F6) in a standard fragmentation test (V50 test)[34]. Other values (325, 975 and 1300 m/s) were also used in order to analyze the effect of speed in the relative ballistic performance of the scaled plates.

The parallelepipedic armour plate has dimensions $120 \times 120 \times 4\,mm^3$—although a few simulations were carried out also in plates with half the thickness ($t = 2$ mm) to evaluate the effect of this parameter—which are within the typical range used for impact testing in ceramics. The alumina plate was segmented into prismatic scales of homogeneous size, with square, hexagonal, circular or rhombic bases. The size for each type of scale was defined as the diameter of the inscribed circumference, *s*, and was varied from 5 to 50 mm in the case of the square tiles in order to analyze the effect of this parameter in the ballistic performance. The tiles are held together by an epoxy adhesive interlayer with a minimum thickness of 0.2 mm. A monolithic alumina plate was also simulated for comparison. Alumina and epoxy are selected as model materials, as they have been widely used in armour applications and their ballistic behaviour has been thoroughly analyzed in the literature [18,35–39].

A general contact scheme was defined where all elements in the model, both from FSP and the segmented alumina/epoxy plate, could interact with each other. Normal '*hard*' contact—which minimizes interpenetration between surfaces and does not transmit tensile forces—and a penalty-enforced, isotropic tangential frictional behaviour with a friction coefficient of 0.2 were selected as the interaction properties for the whole model.

2.2. Mesh

An example of the finite element meshes used in this study is shown in Fig. 3. Linear hexahedral (brick) elements with incompatible modes formulation (C3D8I) were used to simulate the scaled ceramic plate. A fine mesh, with approximately cubic elements of ~0.2 mm side, is used in a central region of 100 mm^2 around the contact and also in the FSP. A slightly coarser mesh (maximum size $\sim 0.4 \times 0.4 \times 0.2\,mm^3$) covers the adjacent surrounding area of ~2500 mm^2, and element size is increased further away to a maximum value of $\sim 1.2 \times 1.2 \times 0.2\,mm^3$, in order to reduce the computational cost. This mesh configuration was selected after a comprehensive convergence study, which showed that any additional mesh refinement produced variations on the projectile exit velocity of less than 2%, in the worst case. The use of elements with incompatible modes enabled a faster convergence of results—and a significant reduction in the artificial energy associated to hourglass control—in this bending-dominated problem. However, this type of elements proved inappropriate for the simulation of the thin interlayer of adhesive, since they yielded unphysical negative elastic strain energies. Consequently, for the simulation of the epoxy films and the FSP (where bending does not occur), linear hexahedral elements with reduced integration (C3D8R) were used instead. The adhesive interlayer mesh matched that of the surrounding scales, but a minimum of four elements was set long its thickness at any point, to minimize any shear locking issues associated to the selection of reduced integration elements. No numerical element distortion control was needed except for the FSP elements, where default ABAQUS configuration was used. Both linear and quadratic bulk viscosity were set to 0.05 to minimize artificial energies (kept well below 2% of the internal energy of the system in all cases).

2.3. Material constitutive models

The FSP is modelled as an elasto-viscoplastic material approximating the properties of hardened tool steel. The

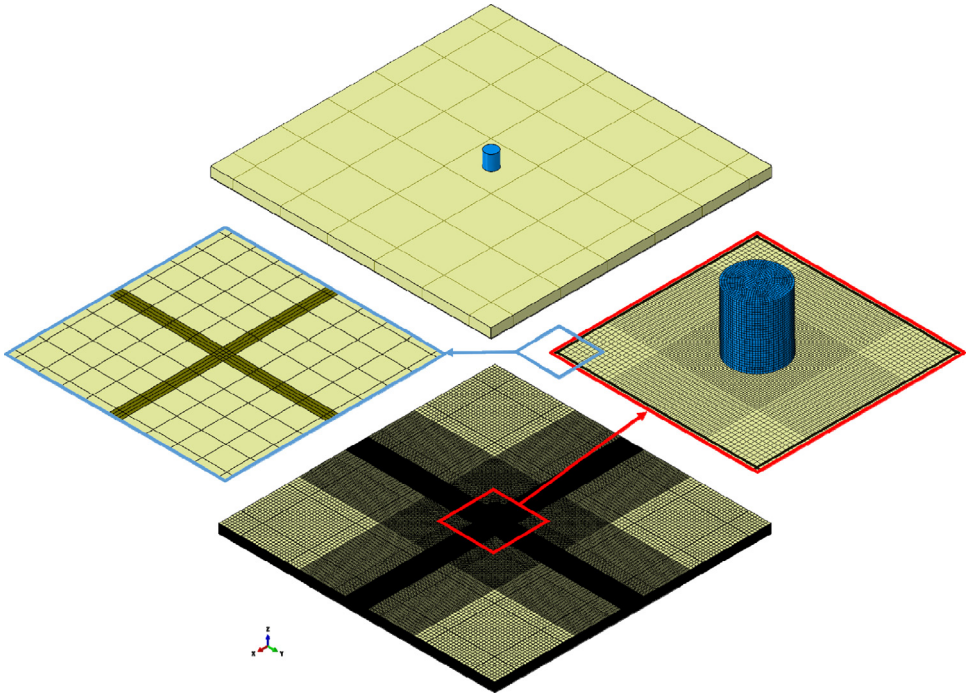

Fig. 3 – Three-dimensional model used to simulate the impact of a cylindrical projectile (FSP) onto the centre of a scaled plate: system overview (top), finite element mesh (bottom), and details of the mesh at impact point (right) and at the adhesive interlayer between scales (left).

Johnson–Cook flow stress model was used simulate the FSP strain-rate dependent plastic behaviour [40]. The parameters used for this empirical model are given in Table 1. The data was derived from existing literature on ballistic simulations involving steel [35,36,41]. A slightly modified value of density was used in order to obtain the desired FSP mass of 1.1 g required by STANAG standard [34].

The ceramic armour is simulated using the Johnson–Holmquist damage model (JH-2) [42], which is typically used for ballistic simulations of ceramics, glass, and other brittle materials [35]. The ABAQUS/Explicit built-in VUMAT user-subroutine for this model was used with parameter values for alumina obtained from literature [35,36], which are summarized in Table 2.

Finally, as demonstrated by López-Puente et al. [37], epoxy adhesive behaviour under ballistic impact conditions can be successfully simulated—given its much lower resistance and modulus—by considering it as a fluid and using Mie–Grüneisen equation of state. Both shear and tensile failure criteria were defined for this material. The parameters used for simulating the epoxy resin in ABAQUS are given in Table 3, as extracted from existing literature [35–37].

For all materials, element deletion was enabled to avoid computational problems associated with excessively distorted elements. Elements were deleted when all their integration points met the failure criteria defined in each of the materials models. In the Johnson-Cook model used for FSP, failure occurs when the damage parameter $\omega \geq 1$. Similarly, the criterion for the Johnson–Holmquist model used for representing alumina, also considers that failure occurs when the equivalent plastic strain (PEEQ) reaches a critical value (see Table 2). Equivalent plastic strain and hydrostatic tensile stress limits are also the criteria for failure in the Mie–Grüneisen EOS-based model used for epoxy, the corresponding limit values are included in Table 3.

Table 1 – Constitutive model (Johnson–Cook) parameters for steel [35,36,41].

Parameter	Symbol	Value	Units
Density	ρ	7.813	kg/m^3
Elastic modulus	E	205	GPa
Poisson's ratio	ν	0.29	
Yield stress	A	792	MPa
Hardening constant	B	510	MPa
Hardening exponent	n	0.26	
Thermal softening exponent	m	1.03	
Melting temperature	T_m	1793	K
Transition temperature	T_{room}	293	K
Strain rate constant	C	0.014	
Reference strain rate	$\dot{\varepsilon}_0'$	0.002	s^{-1}
Johnson–Cook failure parameters	d_1	0.05	
	d_2	3.44	
	d_3	−2.12	
	d_4	0.02	
	d_5	0.61	

2.4. *Evaluated parameters and scope of the study*

Two main parameters were evaluated in the simulations: the amount of damage produced in the ceramic tiles and the final residual velocity of the FSP after impact. The latter parameter was readily obtained as the equivalent rigid-body translational

Table 2 – Constitutive model (Johnson–Holmquist) parameters for alumina.

Parameter	Symbol	Value	Units
Density	ρ_0	3.8	kg/m^3
Shear modulus	G	135	GPa
Normalized intact strength constant	A	0.989	
Normalized intact strength exponent	N	0.367	
Normalized fractured strength constant	B	0.77	
Normalized fractured strength exponent	M	1	
Strain rate dependence parameter	C	0	
Reference strain rate	ε'_0	1	s^{-1}
Maximum hydrostatic tensile stress	T	150	MPa
Maximum normalized intact strength	σ_i^{max}	1	
Maximum normalized fractured strength	σ_f^{max}	0.5	
Net compressive stress at Hugoinot elastic limit	HEL	5.9	GPa
Pressure component at Hugoinot elastic limit	p_{HEL}	2.2	GPa
Elastic to hydrostatic energy loss conversion factor	β	1	
Plastic strain to fracture constant	D_1	0.01	
Plastic strain to fracture exponent	D_2	1	
Maximum failure strain	$\varepsilon_{f,max}^{pl}$	2	
Maximum failure strain	$\varepsilon_{f,min}^{pl}$	0	
Failure criteria (PEEQ > FS)	FS	1.5[a]	
Damage flag (progressive damage, JH-2)	1Damage	0[b]	
Bulk modulus	K_1	200	GPa
Second pressure coefficient	K_2	0	GPa
Third pressure coefficient	K_3	0	GPa

[a] Failure occurs when equivalent plastic strain reaches the limit value.
[b] Progressive damage (JH-2 model).

Table 3 – Constitutive model (Mie–Gruneisen) parameters for epoxy.

Parameter	Symbol	Value	Units
Density	ρ	1.186	kg/m^3
Shear modulus	E	1.6	GPa
Shock equation of state parameter	C	2730	m/s
Shock equation of state parameter	S_1	1.493	
Grüneisen coefficient	γ_0	1.13	
Yield stress	Y	45	MPa
Equivalent plastic strain at failure	ε_f^{pl}	1.5	
Hydrostatic stress tensile limit	T	150	MPa

velocity (VCOM variable in ABAQUS) of the element set constituting the FSP. The amount of damage was evaluated from the corresponding damage contour plots (output variable SDV4 in JH-2 VUMAT subroutine). The size of the damaged zone was estimated as its largest linear dimension, disregarding any damage produced along the external edges of the simulated plate as a consequence of the restrictive boundary conditions imposed there.

At this point, it is worth noting/reminding that the present work is intended as a comparative study of the effect of segmentation in the ballistic performance of a ceramic plate. Therefore, the individual material properties selected, as described in the preceding subsection, and their potential accuracy at representing actual material performance, while already proven in the literature, are of secondary relevance. Indeed, while those material parameters can obviously affect the absolute values obtained for the evaluated ballistic performance parameters described above, they will not qualitatively affect the trends observed upon variation of the different geometrical/testing parameters and, thereby, do not jeopardize the validity of the subsequently derived conclusions.

3. Results and discussion

Fig. 4 shows the damage contours calculated by FEM 0.1 ms after the impact of the cylindrical FSP at 650 m/s onto an unsegmented alumina plate (Fig. 4a) and compares it to the same damage in square-tiled structures with sizes of 20, 10 and 5 mm (Fig. 4b–d). The effectiveness of segmentation as a means to reduce the damage on ceramic plates armour after a ballistic impact is clearly illustrated. Damage in the unsegmented ceramic plate extends over most of its volume, initiating in the form of concentric ring cracks in the front surface, and radial cracks in the back surface of the plate, as typical in bending dominated problems. Some of either type of cracks are eventually able to propagate to the opposing surface in this relatively thin (4 mm) ceramic plate, as shown in Fig. 4a. In the segmented plates, damage is mostly confined to the individual tile hit by the FSP, for the bigger tile sizes (Fig. 4b). This is in good agreement with experimental observations in this type of mosaic armour, at least when a suitable adhesive material is used to bond the plates together [43]. However, at

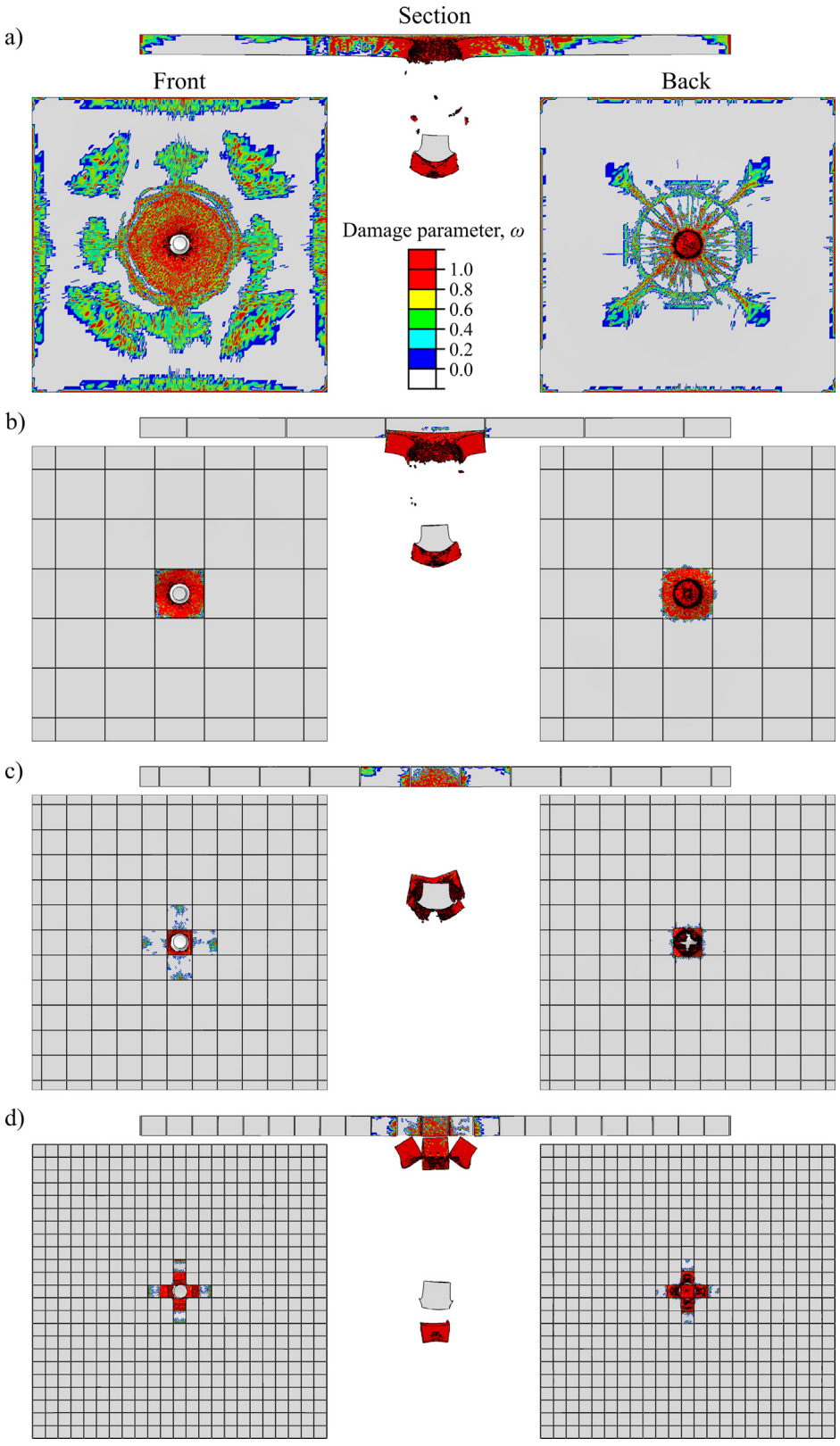

Fig. 4 – Damage contours calculated by FEM 0.1 ms after the impact of the cylindrical FSP at 650 m/s onto (a) an unsegmented alumina plate and square-tiled structures with tile sizes of (b) 20 mm, (c) 10 mm and (d) 5 mm. Front, back and section views of the damage are provided in each case, as indicated in (a).

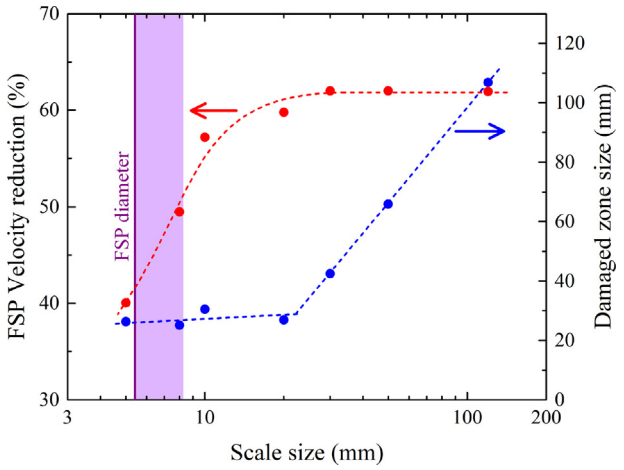

Fig. 5 – Reduction on the FSP velocity upon going through the ceramic plate (left) and size of the damaged zone (right) as a function of the tile size. The rightmost datapoints in these plots represent the values for the unsegmented alumina plate. Vertical shaded band represents the range of variation of FSP diameter during impact. Dashed lines are just visual guidelines.

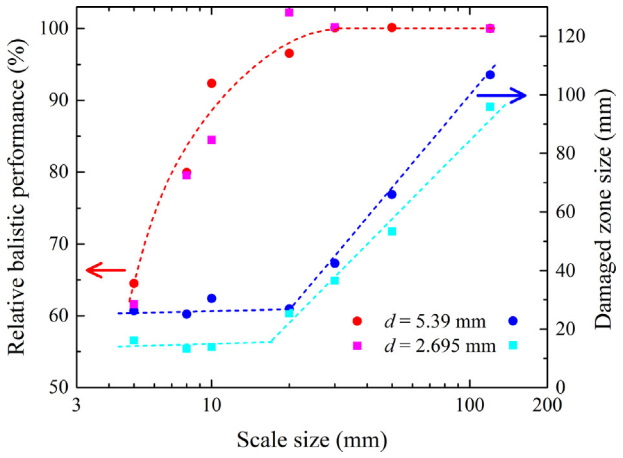

Fig. 6 – Relative ballistic performance (velocity reduction relative to the unsegmented case) of the scaled plates and size of the damage zone after the impact of FSPs of indicated diameters, *d*, as a function of the scale size. Dashed lines are just visual guidelines.

lower sizes, a significant amount of damage is transmitted to adjacent tiles (Fig. 4c and d).

The reduction in the damaged area may come at the expense of a lowering of ballistic protection provided by the plate, as evidenced, for the smaller tiles, by the larger distance travelled (indicating higher exit velocity) by the projectile in the section view of Fig. 4d, compared to that of Fig. 4a. To better analyze these contraposed effects, the reduction of the FSP velocity upon traversing the ceramic plate and the size of the damaged zone are plotted in Fig. 5 as a function of the tile size. The rightmost data points in these plots represent the values for the unsegmented alumina plate: projectile velocity is reduced by nearly 62%—implying that about 85.5% of the kinetic energy of the FSP has been dissipated—and, as depicted in Fig. 4a, the damage extends over most of the size of the monolithic ceramic plate. Upon segmentation, as previously discussed, the damage zone size declines initially fast with the reducing tile size (Fig. 5, right plot), since the damage becomes confined to the individual tile hit by the FSP (Fig. 4b). However, below a certain tile size (~20 mm in the present case), the reduction of the damage zones slows down drastically, virtually stopping, as damage starts to be transmitted to adjacent tiles (Fig. 4c and d). Fortunately, until about precisely this tile size, the FSP velocity reduction achieved by the segmented plates is virtually the same as that of the bulk ceramic. Thus, the scaled armour with 20 mm tiles provides about the same ballistic protection—96.5% in terms of velocity reduction, 98% in terms of kinetic energy reduction, in comparison with the monolithic ceramic plate, while reducing the size of the zone damaged by the impact to a fourth of the unsegmented plate value. This fact demonstrates how little brittle crack propagation contributes to energy dissipation during ballistic impact.

This critical tile size (20 mm) is substantially larger than the diameter of the FSP (5.39 mm), even after deformation during impact; the vertical shaded band in Fig. 5 represents the variation of FSP diameter during impact. In any case, to determine whether the diameter of the FSP affects the critical tile size, simulations were performed using a cylindrical FSP with the same mass but half the initial diameter—by increasing its length by a factor of 4. In Fig. 6, the size of the damage zone and the relative ballistic performance (estimated as the velocity reduction relative to the unsegmented case) of the scaled plates are plotted, for each FSP diameter, as a function of the scale size. The results suggest that reducing the diameter of the projectile seems to decrease somewhat the size of the damage zone produced for a given tile size. This is a direct consequence of the lower ability of the plate to absorb energy from this sharper projectile; the velocity reduction in the unsegmented plate diminishes to ~45% (70.1% kinetic energy reduction), vs. ~62% (85.5%) for the original diameter. However, apparently there is no significant change in the critical tile size upon the reduction of the diameter, since the ballistic performance relative to the unsegmented plate follows closely the same curve for both diameters. Of course, that might change in the case of larger projectiles, especially when the projectile diameter approaches the critical tile size, since impacts close to the inter-scale interfaces may reduce ballistic protection, as will be discussed below. It is obviously, then, a good design guideline to keep tile size larger than the diameter of the projectiles for which the segmented armour is designed, and always above this critical tile size of ~20 mm.

Another geometrical factor that could be determining the value of this key design parameter in a bending-dominated problem, such as this one, is the thickness of the plate. However, while thickness is critical in determining the size of damage zone in static flexural problems [44], this is not the case in dynamic problems, as illustrated by the results on Fig. 7. The size of the damage zone and the relative ballistic performance (i.e. velocity reduction relative to the unsegmented case) of scaled plates of 2 and 4 mm thickness are plotted as a function of the scale size. It is evident that both thickness values yield curves nearly undistinguishable for

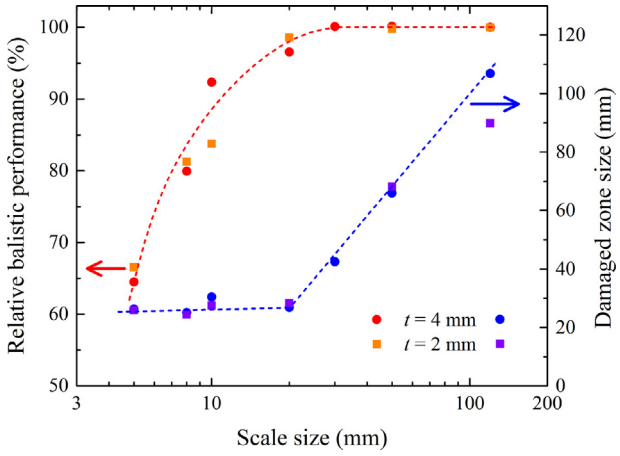

Fig. 7 – Relative ballistic performance (velocity reduction relative to the unsegmented case) of scaled plates of indicated thickness, t, and size of the damage zone after the FSP impact, as a function of the tile size. Dashed lines are just visual guidelines.

both plotted parameters in segmented structures, suggesting that thickness plays no significant role whatsoever in determining the critical tile size.

Projectile speed, on the other hand, does seem to play a significant role in determining how segmentation affects the ballistic performance. Fig. 8 shows the velocity (and kinetic energy) reduction as a function of the FSP velocity for four different tile sizes, *s*. At the highest speed simulated, 1300 m/s, all segmented armours seem to basically yield the same level of ballistic protection (differences well below 10%) as the monolithic plate. Chocron et al. similarly found that the effects of the impact position and the edge distance became lower when the impact velocity increased [45]. This is good news for the effectiveness of the segmentation strategy, since its main potential drawback (the reduction of ballistic protection) seems to be reduced against the most dangerous threats. As the projectile speed is reduced, however, the curve for each tile size progressively separates from that of the unsegmented

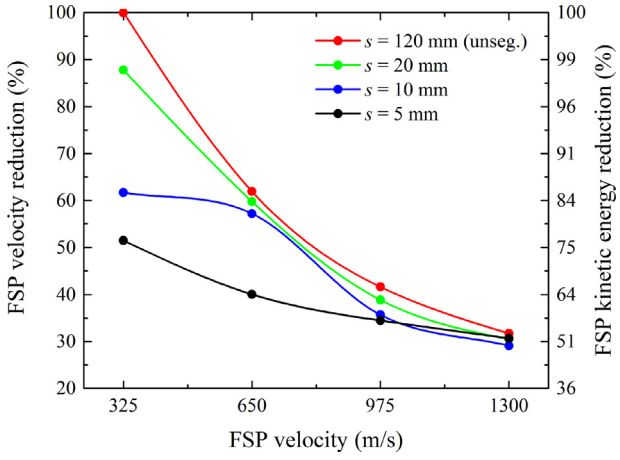

Fig. 8 – Velocity (and kinetic energy) reduction as a function of the FSP velocity for four different tile sizes, *s*. Solid lines are just visual guidelines.

plate. As tile size decreases, this deviation occurs earlier (around 975 m/s, for s = 5 mm, or 650 m/s for s = 10 mm). Even the previously estimated 'safe' size of s = 20 mm starts to provide significantly less protection (~12% less speed reduction) than the unsegmented plate at the lowest speed of 325 m/s. However, since the absolute level of protection provided by the ceramic plates, either segmented or unsegmented, monotonically increases with the reduction in projectile speeds (Fig. 8), a lower speed implies a lower level of threat, and this can be regarded as a minor concern.

The results of Fig. 8, imply that the critical tile size below which ballistic protection starts to decline depends basically on whether the stress waves have enough time to bounce back on the tile sides and significantly contribute to further damaging the ceramic before the bullet perforates the plate on its own. Critical tile size—estimated here at $s \sim 20$ mm for alumina at typical ballistic speeds—will then depend both on the projectile speed and on material properties such as the speed of sound and intrinsic damage resistance: the greater the speed of sound (higher elastic modulus, lower density) and damage resistance of the ceramic, the larger the critical tile size. If this hypothesis is correct, which surely warrants further investigation, it would mean that ceramics with the best ballistic performance would be the most affected by segmentation.

Of course, all the above discussion has been made assuming that impacts occur at the tile centre, while it is highly probable that they occur at (or close to) the interface between plates [33]. It is a priori expected that ballistic protection will be significantly reduced when such interfacial impact occurs, but up to date there were no studies analysing how much the ballistic protection of the segmented plate is reduced when hit at inter-plate boundaries or other locations. Such a study has been performed in this work, not only for the segmented alumina plate with square scales, but also in plates with hexagonal, circular or rhombic prismatic tiles, in order to analyze the effect of scale geometry as well. Size for each type of scale was defined as the diameter of the inscribed circumference, s, and kept constant at the critical size estimated previously for square scales (i.e. s = 20 mm).

Fig. 9 shows the damage contours calculated by FEM 0.1 ms after the impact of the cylindrical FSP onto segmented alumina plates with square (Fig. 9a), hexagonal (Fig. 9b), rhombic (Fig. 9c) and circular (Fig. 9d) scales. This figure evidences that damage produced by an impact right at the centre of a scale is still limited to the impacted scale independently of the scale shape. On the other hand, as expected, when the projectile hits at a corner or at the interface between scales, the damage extends to all tiles impacted. Nonetheless, while the damaged zone seems to extend over most of the tile surfaces at the front, at the back it concentrates into well-defined cracks rather than the complete damage occurring in centred impacts. This is attributed to the alleviation of flexural stresses provided by the interfaces under the contact, which act as pre-existing cracks. Anyhow, even in the most unfavourable case (rhomboidal tile, Fig. 9c) the damaged area is still smaller than in the monolithic plate (Fig. 4a), which again evidences the aptness of segmentation strategy to reduce damage in armour.

The full dependence of the damage zone size on the location of impact for each type of scale is shown in Fig. 10.

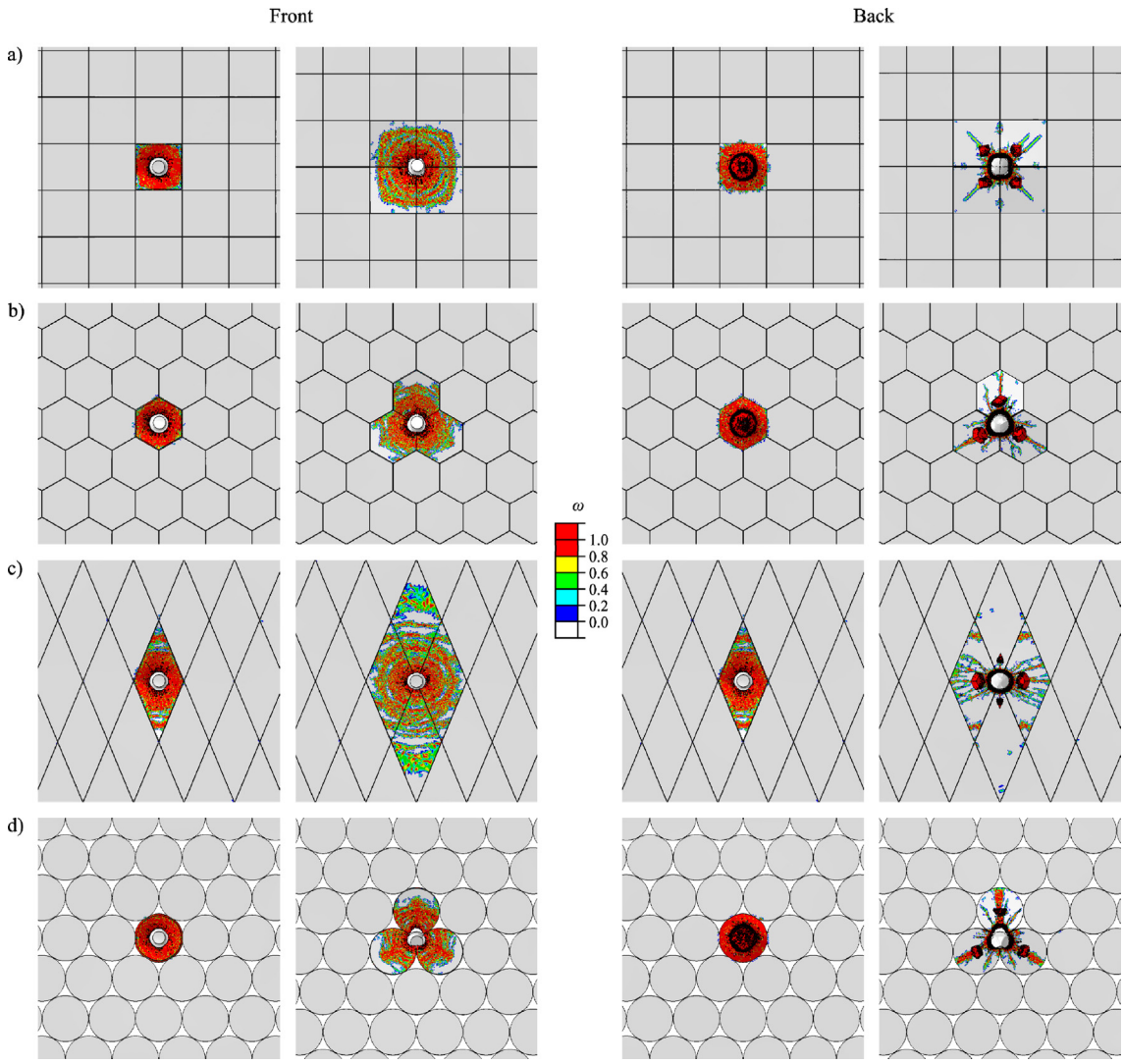

Fig. 9 – Damage contours calculated by FEM 0.1 ms after the impact of the cylindrical FSP at 650 m/s onto segmented alumina plates with (a) square, (b) hexagonal, (c) rhombic and (d) circular scales. Front (left column) and back (right column) views of the damage after impacts at centre (left image within each column) and at the corner/triple points between scales (right images on each column).

Numerical data were obtained for simulated impacts occurring at the locations indicated by open circles, and the full contour plots estimated by using thin plate splines for data interpolation and smoothing. Data are shown for only a quarter of each scale, which contains all the relevant information thanks to the scale symmetry. From these numerical results it is evident that damaged area is maximum when impact occurs at the corner of the plates, as expected. The minimum damage sizes occur in circular plates, followed by hexagonal tiles. Square scales exhibit a larger dependence of the size of the damage produced with the location of the impact, and the rhomboidal shape produces, with difference, the larger damage sizes independently of the impact location. Therefore, damage size—as estimated here by its largest linear dimension—correlates well with the maximum tile dimension. Minimization of the damaged area after each impact seems to call, thus, for rounder tiles, avoiding the use of sharply angled scales.

Regarding the variation of the ballistic performance, Fig. 11 shows contour plots representing the FSP velocity reduction with impact location for the four different tile geometries analyzed. Again, these contour plots were estimated using thin plate splines interpolation from actual data obtained in numerical simulations of impacts occurring at the locations indicated by open circles. Data are shown for a quarter of each scale, making use of segmented scale symmetries. As expected, ballistic protection decreases as the impact location moves away from the tile centre. However, interestingly, the most deleterious location for the impact in terms of affecting the ability of reducing the speed of the projectile is not at the interface between adjacent tiles nor at the corners—although the latter maximizes the size of the damaged area (see Fig. 10). Instead, velocity reduction is minimal when the projectile directly hits a single tile but close to the interface with adjacent scales. In that case tilting of the scale can occur upon failure of the interlayer adhesive, with

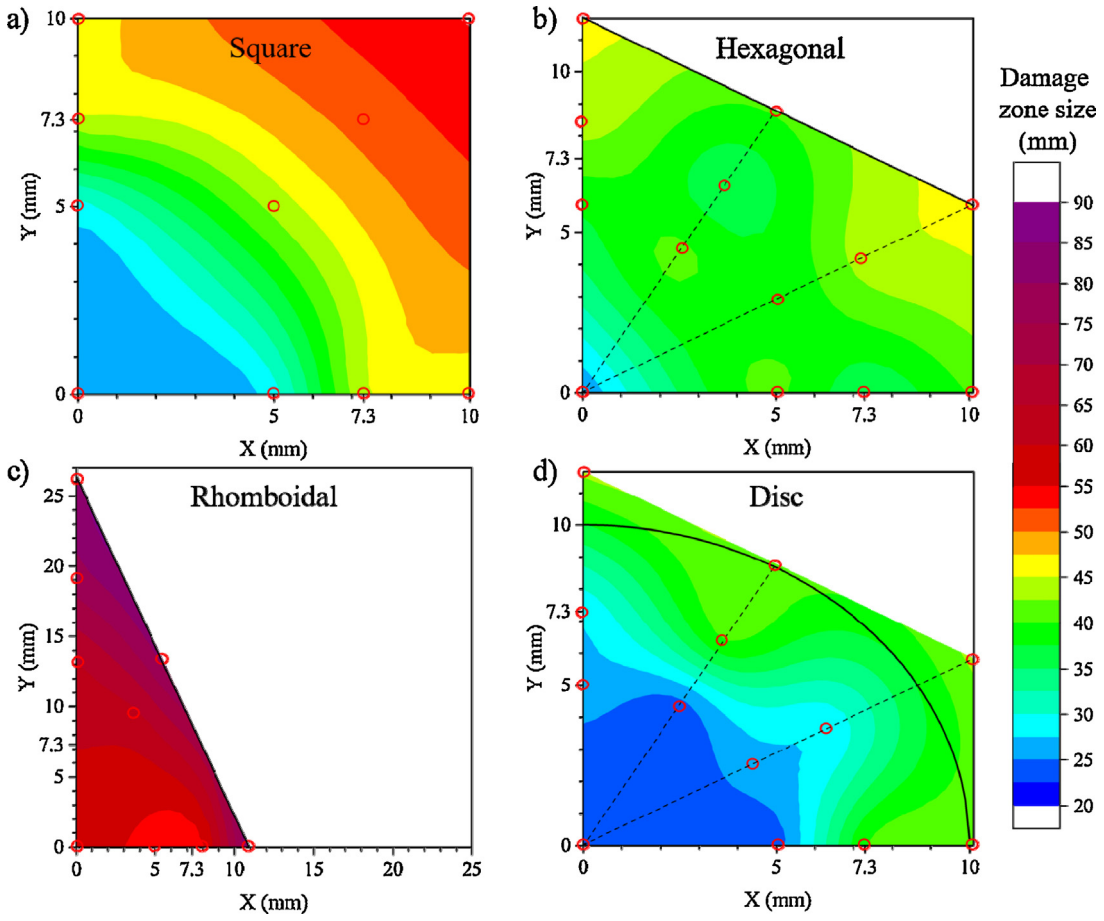

Fig. 10 – Variation of the damage zone size with the location of impact for each type of scale, as indicated. Open circles indicate locations were numerical data was obtained and the full contour were estimated by interpolation and smoothing using thin plate splines. Data is shown for only a quarter of each scale, with (0,0) coordinates corresponding to the centre of each tile.

ensuing reduction of the ballistic protection provided by the segmented armour. The deleterious effect of plate tilting has indeed been previously reported in segmented plates under localized quasi-static loading [23,46]. Selection of an appropriate backplate or using tile overlapping [47] or topological interlocking [48,49] might prove suitable strategies to minimize this problem. In any case, despite the lack of any such preventive measures, the ballistic performance of the segmented armour was not reduced by more than 19% relative to an impact at the tile centre, for any impact location and tile geometry. Among the different geometries, from the results in Fig. 11 it is clear that square tiles and, especially, hexagonal scales provide the most uniform levels of protection: FSP speed reduction decreased by less than 9% and 7% (i.e. ballistic performance was reduced by 15% and 12%), respectively, relative to centred impacts. The reduction of FSP velocity at the tile centre was, within errors, independent of scale geometry, with the sole exception of the disc-shaped tiles, which exhibited significantly (~6%) lower ballistic performance. The latter is attributed to the increased amount of adhesive in the segmented plate, especially at the triple points between the discs. All in all, the segmented armour based in hexagonal scales seems to offer the best overall ballistic performance independently of the impact location; at least against the type of ballistic threat analyzed in this study: they exhibit optimal behaviour in terms of reduction of projectile speed (Fig. 11); and regarding the size of the damaged region they are only surpassed by the disc-tiled armour (Fig. 10), which is the weakest configuration in terms of speed reduction (Fig. 11). The unsuitability of disc shaped tiles for mosaic armours due to its lower ballistic protection, especially against non-centred impacts, has been recently demonstrated experimentally [31]. The regular hexagonal geometry is the closest alternative to a disc shape—which provides minimal damage area for a given tile size after impact—that is capable of fully tessellating the armour plate. This avoids the deleterious effect associated to the excess of weak adhesive in the disc-based alternative. Subsequently, according to the results of this study and in good agreement with nature's preferred designs (Figs. 1 and 2), hexagonal scales are deemed an optimal choice for the fabrication of adhesively-bonded ceramic segmented armours for ballistic protection. Of course, disc scales might become appropriate under other configurations where overlapping is used to remove the armour gaps at the triple points. Overlapping or topologically interlocking the scales, and the use of an appropriate backplate, appear also as promising strategies

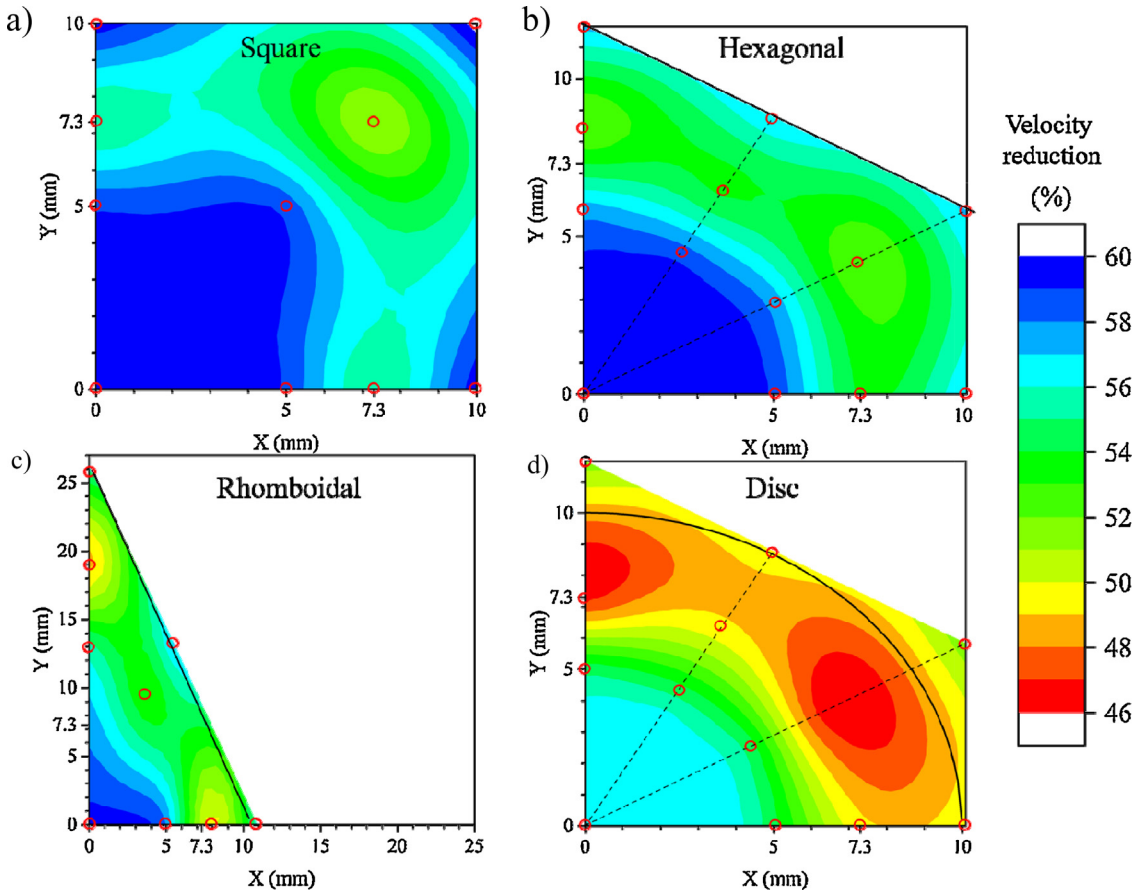

Fig. 11 – Variation of the FSP velocity reduction with the location of impact for each type of scale, as indicated. Open circles indicate locations were numerical data was obtained and the full contour were estimated by interpolation and smoothing using thin plate splines. Data is shown for only a quarter of each scale, with (0,0) coordinates corresponding to the centre of each tile.

to minimize the effect of impact location on the ballistic performance of segmented armour. Nature provides examples of successful overlapping scaled armours [5,9,50], using most of the analyzed scale shapes, including the weakest one in this study, the rhomboid. Fig. 12a shows the alligator gar (*Atractosteus spatula*), a large Mississippi basin fish. Its ganoid scales have this rhombic shape (Fig. 12b). There is very little overlap between these rigid bony scales; their sides are inclined to the surface plane and fit snugly into the neighbouring scale to eliminate any gap, thereby offering improved protection. These scales form arrays that are at a specific angle with the longitudinal fish axis (~55° [5]) in order to accommodate optimally the flexural movement of the fish. Bioinspired rhombic overlapping scales fabricated with zirconia have the potential of being used as body armour (Fig. 12c, adapted from [9, Fig. 19]). Although its performance is not equivalent to the hexagonal scales, this rhombic structure presents advantages regarding flexibility: sliding between the rows of rhombuses can easily satisfy the geometric requirement that one side is shortened while the other becomes longer during bending caused by movement, as occurs in the alligator gar.

The present study provides useful design guidelines for the development of bioinspired ceramic-based scaled armours for the protection of individuals, vehicles or any other structures and devices against ballistic threats. Such segmented armours will provide enhanced performance in terms of compliance and, especially, of resistance against multiple impacts, compared to monolithic ceramic plates.

4. Conclusions

The results of this study demonstrate that segmentation drastically reduces the size of the damaged area after the impact without significantly reducing the ballistic protection in centred impacts. This is true provided the in-plane tile size is greater than a critical value—under the impact conditions analyzed here this critical size was found to be around 20 mm. The critical tile size is found to be independent of the scale thickness, but decreases with projectile speed, meaning that segmentation is a most effective strategy against the most dangerous, high-speed threats. In any case, tiles size should always be kept larger than the projectile size in order to maximize the ballistic protection.

Off-centred impacts in segmented armours involve, as expected, a certain reduction in the ballistic protection and an increase in the damaged area. However, the results from this study suggest that such reduction is not a major one

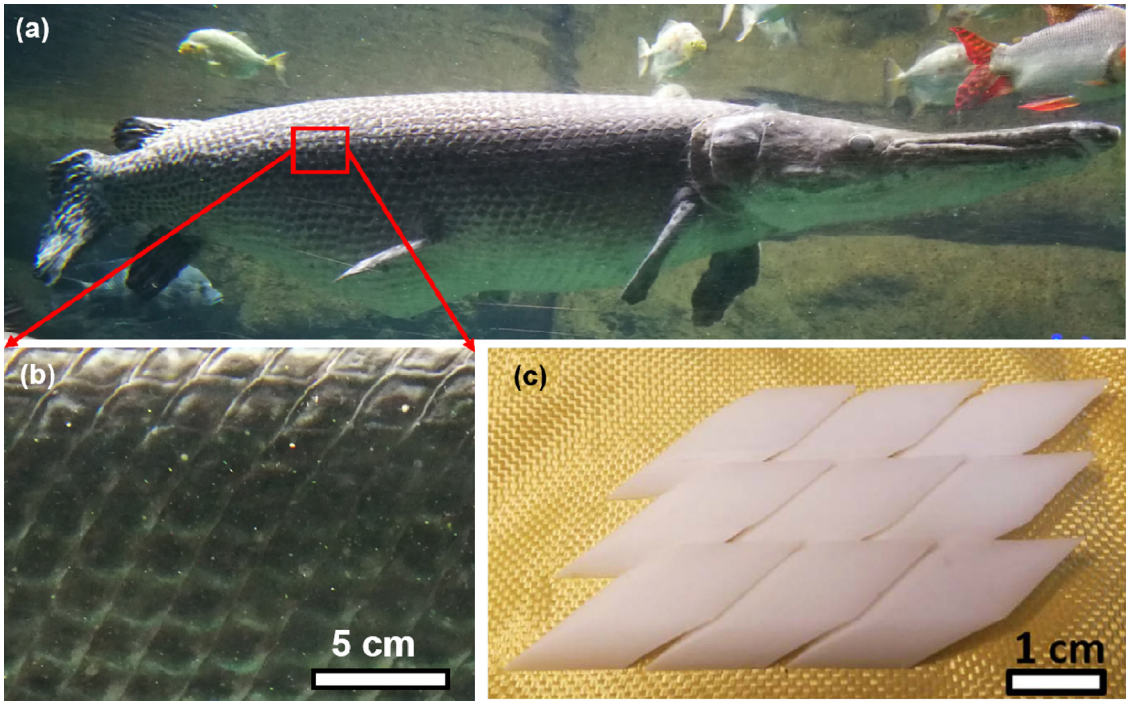

Fig. 12 – (a) Alligator gar (*Atractosteus spatula*), a large Mississippi basin fish; (b) ganoid scales having a rhombic shape. These is very little overlap between these rigid bony scales; their sides are inclined to surface plane to provide improved protection; they form arrays that are at specific angle with the longitudinal fish axis (~55°); (c) bioinspired scales fabricated with zirconia with potential application as body armour (adapted from [9, Fig. 19]).

(well under 20% for all the conditions evaluated in this work). Moreover, an appropriate selection of the tiles shape can significantly reduce this problem and, in this sense, among the shapes analyzed, hexagonal scales provide the best performance with a ballistic protection that decreased by less than 12% at the worst impact location. This corroborates the geometry of natural tiles present in the carapace of armadillo [4] and boxfish [5,6] (Figs. 1 and 2), which has been selected by nature through a convergent evolution process, is also the one offering best ballistic protection.

Conflicts of interest

The authors declare no conflicts of interest.

Acknowledgements

This work was supported by the Ministerio de Educación Cultura y Deporte, Spain [grant PRX16/00125], by the Ministerio de Economía y Competitividad, Spain [grant MAT2015-64670-R (MINECO/FEDER)], and by the Junta de Extremadura, Spain [grant IB16094] and co-funded by the European Union through the European Regional Development Fund. This work is also funded in part by the AFOSR MURI (AFOSR-FA9550-15-1-0009). We thank Dr. Wen Yang for kindly preparing the animal specimens and photographing them.

REFERENCES

[1] Yang W, Chen IH, Bernd G, Zimmermann EA, Ritchie RO, Meyers MA. Natural flexible dermal armor. Adv Mater 2013;25:31–48.
[2] Meyers MA, McKittrick J, Chen P. Structural biological materials: critical mechanics–materials connections. Science 2013;339:773–9.
[3] Naleway SE, Porter MM, Joanna M, Meyers MA. Structural design elements in biological materials: application to bioinspiration. Adv Mater 2015;27:5455–76.
[4] Yang W, Gludovatz B, Zimmermann EA, Bale HA, Ritchie RO, Meyers MA. Structure and fracture resistance of alligator gar (*Atractosteus spatula*) armored fish scales. Acta Biomater 2013;9:5876–89.
[5] Sherman VR, Yaraghi NA, Kisailus D, Meyers MA. Microstructural and geometric influences in the protective scales of *Atractosteus spatula*. J R Soc Interface 2016:13.
[6] Wang B, Yang W, Sherman VR, Meyers MA. Pangolin armor: overlapping, structure, and mechanical properties of the keratinous scales. Acta Biomater 2016;41:60–74.
[7] Song J, Ortiz C, Boyce MC. Threat-protection mechanics of an armored fish. J Mech Behav Biomed Mater 2011;4:699–712.
[8] Lin YS, Wei CT, Olevsky EA, Meyers MA. Mechanical properties and the laminate structure of *Arapaima gigas* scales. J Mech Behav Biomed Mater 2011;4:1145–56.
[9] Sherman VR, Quan H, Yang W, Ritchie RO, Meyers MA. A comparative study of piscine defense: the scales of *Arapaima gigas*, *Latimeria chalumnae* and *Atractosteus spatula*. J Mech Behav Biomed Mater: Biol Articulat Struct Prot Des 2017;73:1–16.
[10] Chen IH, Kiang JH, Correa V, Lopez MI, Chen P, McKittrick J, et al. Armadillo armor: mechanical testing and

micro-structural evaluation. J Mech Behav Biomed Mater 2011;4:713–22.
[11] Yang W, Nguyen V, Porter MM, Meyers MA, McKittrick J. Structural characterization and compressive behavior of the boxfish horn. In: McKittrick JM, Narayan R, editors. Advances in bioceramics and biotechnologies II. Hoboken, NJ: Wiley & Sons; 2014. p. 105–12.
[12] Yang W, Naleway SE, Porter MM, Meyers MA, McKittrick J. The armored carapace of the boxfish. Acta Biomater 2015;23:1–10.
[13] Travis H. Roman body armour. Amberley Publishing; 2012.
[14] Decker MJ, Halbach CJ, Nam CH, Wagner NJ, Wetzel ED. Stab resistance of shear thickening fluid (STF)-treated fabrics. Compos Sci Technol 2007;67:565–78.
[15] Atanasov SE, Oldham CJ, Slusarski KA, Taggart-Scarff J, Sherman SA, Senecal KJ, et al. Improved cut-resistance of Kevlar® using controlled interface reactions during atomic layer deposition of ultrathin (50 A) inorganic coatings. J Mater Chem A 2014;2:17371–9.
[16] Wilhelm M, Bir C. Injuries to law enforcement officers: the backface signature injury. Forensic Sci Int 2008;174:6–11.
[17] den Reijer PC, PhD thesis Impact on ceramic faced armour. The Netherlands: Delft Technical University; 1991.
[18] Sherman D. Impact failure mechanisms in alumina tiles on finite thickness support and the effect of confinement. Int J Impact Eng 2000;24:313–28.
[19] Broos JPF, Gunters R. Study on the ballistic performance of monolithic ceramic plates; 2017. p. 1561–7.
[20] Monteiro SN, Lima EP, Louro LH, da Silva LC, Drelich JW. Unlocking function of aramid fibers in multilayered ballistic armor. Metall Mater Trans A 2015;46:37–40.
[21] Sarva S, Nemat-Nasser S, McGee J, Isaacs J. The effect of thin membrane restraint on the ballistic performance of armor grade ceramic tiles. Int J Impact Eng 2007;34:277–302.
[22] Florence AL. Interaction of projectiles and composite armour – Part II. Report AMRA CR 67-05 (F). Stanford Research Institute; 1969.
[23] Chintapalli RK, Mirkhalaf M, Dastjerdi AK, Barthelat F. Fabrication, testing and modeling of a new flexible armor inspired from natural fish scales and osteoderms. Bioinspir Biomim 2014;9:036005.
[24] Larsen J, Cross C. Composite segmented flexible armor. US Patent 2007; US20070234458 A1.
[25] Patel PJ, Hsieh AJ, Gilde GA. Improved low-cost multi-hit transparent armor. In: Army Research Report. US Army Research Laboratory; 2006. ADA481074.
[26] Neal ML, Bain AD. Method and apparatus for defeating high-velocity projectiles [17]. US Patent 2001; US 6170378 B1.
[27] Drelich AJ, Monteiro SN, Brookins J, Drelich JW. Fish skin: a natural inspiration for innovation. Adv Biosyst 2018;2:1800055.
[28] Fejdyś M, Kośla K, Kucharska-Jastrząbek A, Landwijt M. Hybride composite armour systems with advanced ceramics and ultra-high molecular weight polyethylene (UHMWPE) fibres. Fibres Textiles Eastern Eur 2016;24:79–89.
[29] Kim HW, Deng Y, Miranda P, Pajares A, Kim DK, Kim HE, et al. Effect of flaw state on the strength of brittle coatings on soft substrates. J Am Ceram Soc 2001;84:2377–84.
[30] Martinez-Vazquez FJ, Perera FH, Miranda P, Pajares A, Guiberteau F. Improving the compressive strength of bioceramic robocast scaffolds by polymer infiltration. Acta Biomater 2010;6:4361–8.
[31] Hu D, Zhang Y, Shen Z, Cai Q. Investigation on the ballistic behavior of mosaic SiC/UHMWPE composite armor systems. Ceram Int 2017;43:10368–76.
[32] Hazell PJ, Roberson CJ, Moutinho M. The design of mosaic armour: the influence of tile size on ballistic performance. Mater Des 2008;29:1497–503.
[33] Bless SJ, Jurick DL. Design for multi-hit capability. Int J Impact Eng 1998;21:905–8.
[34] STANAG 2920 PPS – ballistic test method for personal armour materials and combat clothing. 2nd ed. NATO Standardization Agency; 2003. A-1.
[35] Rashed A, Yazdani M, Babaluo AA, Hajizadeh Parvin P. Investigation on high-velocity impact performance of multi-layered alumina ceramic armors with polymeric interlayers. J Compos Mater 2016;50:3561–76.
[36] Prakash A, Rajasankar J, Anandavalli N, Verma M, Iyer NR. Influence of adhesive thickness on high velocity impact performance of ceramic/metal composite targets. Int J Adhes Adhes 2013;41:186–97.
[37] López-Puente J, Arias A, Zaera R, Navarro C. The effect of the thickness of the adhesive layer on the ballistic limit of ceramic/metal armours. An experimental and numerical study. Int J Impact Eng 2005;32:321–36.
[38] Medvedovski E. Alumina ceramics for ballistic protection. Part 1. Am Ceram Soc Bull 2002;81:27–32.
[39] Medvedovski E. Alumina ceramics for ballistic protection. Part 2. Am Ceram Soc Bull 2002;81:45–50.
[40] Johnson GR, Cook WH. A constitutive model and data for metals subjected to large strains, high strain rates and high temperatures, vol. 54; pp. 31–48.
[41] Chi R, Serjouei A, Sridhar I, Tan GEB. Ballistic impact on bi-layer alumina/aluminium armor: a semi-analytical approach. Int J Impact Eng 2013;52:37–46.
[42] Johnson GR, Holmquist TJ. An improved computational constitutive model for brittle materials. AIP Conf Proc 1994;309:981.
[43] Jiusti J, Kammer EH, Neckel L, Lóh NJ, Trindade W, Silva AO, et al. Ballistic performance of Al_2O_3 mosaic armors with gap-filling materials. Ceram Int 2017;43:2697–704.
[44] Chai H, Lawn BR. Fracture modes in brittle coatings with large interlayer modulus mismatch. J Mater Res 1999;14:3805–17.
[45] Chocron IS, Anderson CE, Behner T, Hohler V. Lateral confinement effects in long-rod penetration of ceramics at hypervelocity. Int J Impact Eng 2006;33:169–79.
[46] Martini R, Barthelat F. Stability of hard plates on soft substrates and application to the design of bioinspired segmented armor. J Mech Phys Solids 2016;92:195–209.
[47] Roberto Martini FB. Stretch-and-release fabrication, testing and optimization of a flexible ceramic armor inspired from fish scales. Bioinspir Biomim 2016;11:066001.
[48] Estrin Y, Dyskin AV, Pasternak E. Topological interlocking as a material design concept. Mater Sci Eng C 2011;31:1189–94.
[49] Siegmund T, Barthelat F, Cipra R, Habtour E, Riddick J. Manufacture and mechanics of topologically interlocked material assemblies. Appl Mech Rev 2016;68:040803–15.
[50] Martini R, Balit Y, Barthelat F. A comparative study of bio-inspired protective scales using 3D printing and mechanical testing. Acta Biomater 2017;55:360–72.